Coupled-wave analysis of apodized volume gratings

J.M. Tsui and C. Thompson
University of Massachusetts-Lowell, Lowell, MA 01854
email: jtsui@uml.edu

V. Mehta and Jeffrey M. Roth
MIT Lincoln Laboratory, Lexington, MA 02420

V.I. Smirnov and L.B. Glebov
University of Central Florida, CREOL, Orlando, FL

Abstract: This work presents the use of longitudinal refractive index modulation (apodization) in photosensitive glass for improved sidelobe suppression in volume holographic optical elements. We develop a numerical model for both uniform and apodized volume holograms based on rigorous coupled-wave analysis. We validate the model by comparison with a transmissive 1.55-μm uniform volume grating in photothermorefractive glass. We then apply our numerical model to calculate the spectral response of apodized gratings. The numerical results demonstrate that apodization of the refractive index modulation envelope improves spectral selectivity and reduces first and second-order side-lobe peaks by up to 33 and 65 dB, respectively. We suggest a method for creating apodization in volume holograms with approximately Gaussian spatial refractive index profile.

OCIS codes: (090.2890) Holographic optical elements; (090.7330) Volume holographic gratings; (220.1230) Apodization; (260.2110) Electromagnetic theory

References and links

1. A.D. Cohen, M.C. Parker, R.J. Mears, "100-GHz-resolution dynamic holographic channel management for WDM," IEEE Phot. Tech. Lett., **11**, 851-3 (1999).
2. D.C. O'Brien, R.J. Mears, T.D. Wilkinson and W.A. Crossland, "Dynamic holographic interconnects that use ferroelectric liquid-crystal spatial light modulators", Appl. Opt. **33**, 2795-2803 (1994).
3. A. Marrakchi and K. Rastani, "Free-space holographic grating interconnects", *Photonics Switching and Interconnects*, A. Marrakchi (ed.), Marcel Dekker, New York, 249-321 (1994).
4. P.F. McManamon, T.A. Dorschner, D.L. Corkum, L.J. Friedman, D.S. Hobbs, M. Holz, S. Liberman, H.Q. Nguyen, D.P. Resler, R.C. Sharp and E.A. Watson, "Optical phased array technology", Proc. of the IEEE **84**, 268-298 (1996).
5. O.M. Efimov, L.B. Glebov, L.N. Glebova, K.C. Richardson, and V.I. Smirnov, "High-efficiency Bragg gratings in photothermorefractive glass", Appl. Opt. **38**, 619-27 (1999).
6. I.V. Ciapurin, L.B. Glebov, L.N. Glebova, V.I. Smirnov and E.V. Rotari, " Incoherent combining of 100-W Yb-fiber laser beams by PTR Bragg grating", In Advances in Fiber Devices, L. N. Durvasula, Editor, Proceedings of SPIE **4974**, 209-219 (2003).
7. S. Tao and G.W. Burr, "Performance optimization of volume gratings with finite size through numerical simulation", *CLEO/IQEC and PhAST Technical Digest* (Optical Society of America, Washington, DC, 2004), CTuE5.
8. T. K. Gaylord and M.G. Moharam, "Planar Dielectric Grating Diffraction Theories", Appl. Phys. B **28**, 1-14 (1982).
9. L.B. Glebov, "Kinetics modeling in photosensitive glass," Optical Materials **25**, 413-418 (2004).

#5752 - $15.00 US Received 23 November 2004; revised 16 December 2004; accepted 16 December 2004

10. M.G. Moharam and T.K. Gaylord, "Rigorous coupled-wave analysis of planar-grating diffraction," J. Opt. Soc. Am. **71**, 811-818 (1981).
11. T.K. Gaylord and M.G. Moharam, "Analysis of optical diffraction by gratings", Proc. of the IEEE **73**, 894-937 (1985).
12. K. Radhakrishnan and A.C. Hindmarsh, "Description and use of LSODE, the Livermore Solver for Ordinary Differential Equations", NASA reference publication 1327 (1993).
13. G.D. Byrne and A.C. Hindmarsh, "Stiff ODE solvers: A review of current and coming attractions", J. Comp. Phys. **70**, 1-62 (1987).

1. Introduction

Several practical applications exist in optical communications for holographic optical elements. The narrow-band diffractive property of holograms can be exploited in wavelength-division multiplexed optical systems as channel-drop filters and equalizers [1] and as reconfigurable multi-wavelength optical cross-connect switches [2, 3]. Holographic elements also enable a lightweight, wavelength-selective alternative to mechanical gimbals for optical beam-steering in free-space optical communications [4]. As an extension of this approach, a cascade of multiple holograms in series could enable a single aperture to independently steer multiple users contained within a wavelength-multiplexed beam. Furthermore, volume holograms enable synthesis of advanced filter shapes that cannot be easily achieved with interference filters. In addition to dynamic, spatial light modulator approaches to generating holograms, experimental demonstrations of fixed, sinusoidal volume holograms in photothermorefractive (PTR) glass show these gratings achieve diffraction efficiencies near 100%, accomodate high power, and exhibit low loss at communication wavelengths near 1.55 μm [5, 6].

An area for further investigation involves improving the spectral response of sinusoidal volume gratings. A typical transmissive uniform volume grating with $\sim$1-mm thickness exhibits sidelobes and a response that decays by approximately -20 dB per 15 nm at 1.55 μm. We propose the use of apodization of the refractive index modulation amplitude to enhance the stop-band rejection of a volume grating. The use of apodization (or spatially non-uniform coupling) in gratings has also recently been proposed in Ref. [7]. They have provided numerical results for the spectral response of gratings apodized with a Sinc-profile using integration of approximate coupled-wave equations for finite beams. In this work, we address the problem of oblique plane-wave diffraction from an apodized volume grating using a rigorous derivation of the coupled-wave equations stemming from analysis developed by Gaylord and Moharam [8]. We develop a numerical solution for the set of coupled-wave equations governing the spatial variation of the electric field, and validate our numerical solution with measurements of an experimental uniform grating device. We then apply our numerical approach to calculating the spectral response of apodized gratings. The use of a Gaussian profile for apodization is found to allow considerable side-lobe suppression in the grating's spectral response, while preserving the main-lobe bandwidth. We show through numerical calculations that first and second-order side-lobe peaks can be reduced by 33 and 65 dB, respectively. This improvement corresponds to a stop-band response with 80 dB of suppression at a detuning of under 0.7% relative to the grating's center wavelength. A simple model for fabrication of nearly Gaussian spatial index profile is accomplished by exploiting spectral properties [5] and kinetics of refractive index modification [9] in PTR glass.

The content of the remainder of this paper includes the derivation of the coupled-wave equations for an apodized grating in Section 2. In Section 3 we describe our numerical solution approach and in Section 5 we present the results of our numerical solution. A summary of our work and conclusions are given in Section 6.

#5752 - $15.00 US Received 23 November 2004; revised 16 December 2004; accepted 16 December 2004

2. Coupled-wave equations

In this section we present the derivation of the coupled-wave equations for wave propagation through an apodized grating. The grating and its bounding media are assumed to be linear and isotropic. The evolution of the electric field, $\bar{E}$, is given by the following vector-wave equation.

$$\nabla^2\bar{E} + \nabla\cdot\left(\frac{\bar{E}\cdot\nabla\varepsilon}{\varepsilon}\right) - \mu\varepsilon\frac{\partial^2\bar{E}}{\partial t^2} = 0 \tag{1}$$

The permeability μ assumes its free-space value μ_0, and the permittivity $\varepsilon(x,z) = \varepsilon_0\tilde{\varepsilon}(x,z)$ varies with position. The quantity ε_0 is the value of permittivity in free-space, and $\tilde{\varepsilon}(x,z)$ is the relative permittivity of the medium. Our analysis here considers only the H-mode polarization of the electric field. The electric field is expressed as a time-harmonic transverse wave with frequency ω: $\bar{E} = \hat{y}E_y(x,z)e^{-j\omega t}$, where $\hat{y}$ is the unit vector in the y-direction. This expression for the electric field forces the second term of Eq. (1), $\nabla\cdot(\bar{E}\cdot\nabla\varepsilon/\varepsilon)$, to be identically zero. Applying this time-harmonic form of the electric field to Eq. (1) results in the following scalar Helmholtz equation for $E_y(x,y)$,

$$\nabla^2 E_y(x,z) + k^2\tilde{\varepsilon}(x,z)E_y(x,z) = 0 \tag{2}$$

where $k = \omega(\mu_0\varepsilon_0)^{1/2}$ is the magnitude of the free-space wave-number, and $\lambda = 2\pi/k$ is the corresponding free-space wavelength.

In our analysis we consider the problem of a planar dielectric grating bound between different homogeneous media, as illustrated in Fig. 1. The dielectric grating is characterized by a relative permittivity, $\tilde{\varepsilon}_2$, that is a superposition of constant and varying components:

$$\tilde{\varepsilon}_2(x,z) = \tilde{\varepsilon}_{20} + \tilde{\varepsilon}_{21}(z)\cos[\bar{K}\cdot\bar{x}] \tag{3}$$

In Eq. (3) $\bar{x} = (x\ y\ z)^T$ is the position vector, and $\bar{K} = K(\sin\phi\ 0\ \cos\phi)^T$ is the grating vector. The angle ϕ is the grating slant angle and $K = 2\pi/\Lambda$ is the magnitude of the grating vector, with the grating period Λ. The quantities $\tilde{\varepsilon}_{20}$ and $\tilde{\varepsilon}_{21}$ denote the mean relative permittivity and the amplitude of the modulated relative permittivity. The spatial variation of the quantity $\tilde{\varepsilon}_{21}(z)$ provides apodization of the sinusoidal modulation of the permittivity.

We are interested in accurately computing the forward and backward propagating diffracted fields that result from a plane wave at oblique incidence to the planar grating. We therefore employ a representation of the solution in terms of the diffracted orders, proposed by Gaylord and Moharam [8, 10, 11]. Following the analysis of Gaylord and Moharam, the electric field inside the grating is expressed as a superposition of spatial harmonics with phase $\bar{k}_{2m}\cdot\bar{x}$ and amplitude, $S_m(z)$.

$$E_{2y}(x,z) = \sum_{m=-\infty}^{+\infty} S_m(z)\exp(-j\bar{k}_{2m}\cdot\bar{x}) \tag{4}$$

The spatial harmonics are parameterized by their wave-vectors, $\bar{k}_{2m} = \bar{k}_2 - m\bar{K}$, where $\bar{k}_2$ is the reference wave-vector with magnitude $k(\tilde{\varepsilon}_{20})^{1/2}$ and m is the integral spatial harmonic index. Substituting Eq. (4) into the scalar Helmholtz equation, Eq. (2), results in the set of second-order coupled ordinary differential equations for the amplitudes $S_m(z)$,

$$S_m'' + \sum_n a_{mn}\,S_n' + \sum_n b_{mn}\,S_n = 0 \tag{5}$$

#5752 - $15.00 US Received 23 November 2004; revised 16 December 2004; accepted 16 December 2004

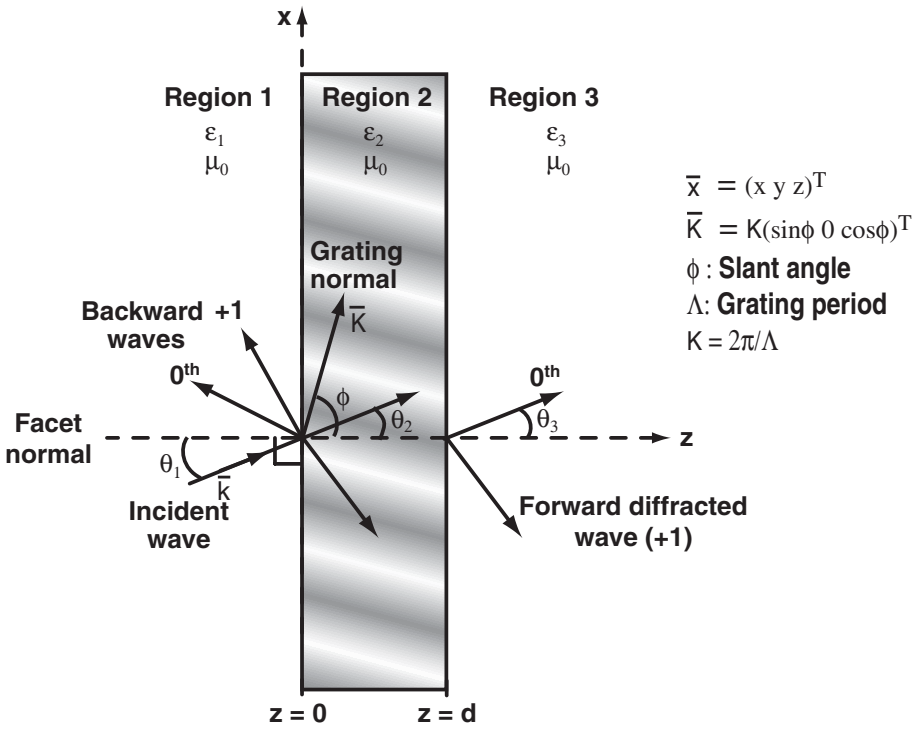

Fig. 1: Diffraction from a planar dielectric grating bounded by homogeneous media.

where $()'$ denotes a derivative with respect to z. The coefficients a_{mn} and b_{mn} are defined as:

$$a_{mn} = \begin{cases} -2j(\bar{k}_{2n}\cdot\hat{z}) & \text{if } n=m \\ 0 & \text{if } n\neq m \end{cases} \tag{6}$$

$$b_{mn} = \begin{cases} [k_2^2-(\bar{k}_{2n}\cdot\hat{x})^2-(\bar{k}_{2n}\cdot\hat{z})^2] & n=m \\ k^2\tilde{\varepsilon}_{21}(z)/2 & n=m-1 \text{ or } n=m+1 \\ 0 & \text{otherwise} \end{cases} \tag{7}$$

$\hat{x}$ and $\hat{z}$ are unit vectors in the x and z directions respectively. The electric field in Regions 1 and 3 are given below.

$$E_{1y} = \exp(-j\bar{k}_1\cdot\bar{x}) + \sum_{m=-\infty}^{\infty} R_m \exp(-j\bar{k}_{1m}\cdot\bar{x}) \tag{8}$$

$$E_{3y} = \sum_{m=-\infty}^{\infty} T_m \exp(-j\bar{k}_{3m}\cdot(\bar{x}-d\hat{z})) \tag{9}$$

The x-components of the wave-vectors $\bar{k}_{1m}$ and $\bar{k}_{3m}$ are obtained by applying phase matching conditions:

$$(\bar{k}_{1m}\cdot\hat{x}) = (\bar{k}_{2m}\cdot\hat{x}) = (\bar{k}_{3m}\cdot\hat{x}) \tag{10}$$

#5752 - $15.00 US Received 23 November 2004; revised 16 December 2004; accepted 16 December 2004

The magnitudes of the wave-vectors in the Regions 1 and 3 are $k_1 = |\bar{k}_1| = |\bar{k}_{1m}| = k(\tilde{\varepsilon}_{10})^{1/2}$ and $k_3 = |\bar{k}_3| = |\bar{k}_{3m}| = k(\tilde{\varepsilon}_{30})^{1/2}$, respectively. The z-components of the wave-vectors $\bar{k}_{1m}$ and $\bar{k}_{3m}$ are therefore given as:

$$(\bar{k}_{1m} \cdot \hat{z}) = -\left[k_1^2 - (\bar{k}_{2m} \cdot \hat{x})^2\right]^{1/2}$$
$$(\bar{k}_{3m} \cdot \hat{z}) = +\left[k_3^2 - (\bar{k}_{2m} \cdot \hat{x})^2\right]^{1/2} \tag{11}$$

The quantities R_m in Eq. (8) are amplitudes of the backward-propagating diffracted orders, and T_m in Eq. (9) are the amplitudes of the forward-propagating orders. These amplitudes are specified by conditions on the electrical and magnetic fields at the grating boundaries. The continuity of the tangential electrical and magnetic fields at $z = 0$ and $z = d$ yields the following relations:

$$(\bar{E})_t(z=0): \qquad S_m(0) - \delta_{0m} = R_m \tag{12}$$
$$(\bar{H})_t(z=0): \qquad -j[k_1^2 - (\bar{k}_{2m} \cdot \hat{x})^2]^{1/2}(\delta_{0m} - R_m) = S_m'(0) - j(\bar{k}_{2m} \cdot \hat{z})S_m(0) \tag{13}$$
$$(\bar{E})_t(z=d): \qquad S_m(d)\exp[-j(\bar{k}_{2m} \cdot \hat{z})d] = T_m \tag{14}$$
$$(\bar{H})_t(z=d): \qquad j[S_m'(d) - j(\bar{k}_{2m} \cdot \hat{z})S_m(d)]\exp[-j(\bar{k}_{2m} \cdot \hat{z})d] = (\bar{k}_{3m} \cdot \hat{z})T_m \tag{15}$$

We use the notation $()_t$ to denote the vector component tangential to the grating surface, and δ_{0m} is the Kronecker delta function. The Eqs. (11-14) simplify to the following equations which are independent of R_m and T_m:

$$S_m'(0) - j\left\{(\bar{k}_{2m} \cdot \hat{z}) + \left[k_1^2 - (\bar{k}_{2m} \cdot \hat{x})^2\right]^{1/2}\right\} S_m(0) = -2j\left[k_1^2 - (\bar{k}_{2m} \cdot \hat{x})^2\right]^{1/2} \delta_{0m} \tag{16}$$
$$S_m'(d) - j\left[(\bar{k}_{2m} \cdot \hat{z}) - (\bar{k}_{3m} \cdot \hat{z})\right] S_m(d) = 0 \tag{17}$$

The electric field inside the grating (Region 2) can be obtained by calculating the amplitudes $S_m(z)$ by solving Eq. (5), subject to the boundary conditions in Eqs. (16-17).

3. Numerical solution

Our main interest is in examining the coupling between the spatial harmonics $S_m(z)$ which results in transfer of energy from the incident wave to the forward propagating diffracted orders. It is apparent from Eq. (5) that the coupling between the spatial harmonics is mediated by the modulated component of the relative permittivity $\tilde{\varepsilon}_{21}(z)\cos(\bar{K} \cdot \bar{x})$ (see equation (3)). In the following we show that appropriate selection of the functional form for $\tilde{\varepsilon}_{21}(z)$ allows the spectral selectivity of a sinusoidal grating to be significantly enhanced.

The spatial dependence of the amplitude $\tilde{\varepsilon}_{21}(z)$ renders Eq. (5) inhomogeneous. A general analytic solution to the inhomogeneous coupled differential equations is non-trivial. In this section we seek a numerical solution for the coupled inhomogeneous differential equations that govern the amplitudes $S_m(z)$. The numerical results presented here are limited to a single functional form for $\tilde{\varepsilon}_{21}(z)$. In order to discuss our solutions in terms of familiar optical quantities, we replace relative permittivities with refractive indices. This is accomplished by rewriting Eq. (3) as

$$\tilde{\varepsilon}_{20} + \tilde{\varepsilon}_{21}(z)\cos[\bar{K} \cdot \bar{x}] \approx n_{20}^2 + 2n_{20}n_{21}f(z)\cos[\bar{K} \cdot \bar{x}] \tag{18}$$

where n_{20} is the mean refractive index in, n_{21} is the relative amplitude for the modulated component of the refractive index, and $f(z)$ is the apodization function. In this study we employ

#5752 - $15.00 US Received 23 November 2004; revised 16 December 2004; accepted 16 December 2004

the Gaussian function $G(z;\alpha,\sigma_q)$ to describe the apodization $f(z)$. The function $G(z;\alpha,\sigma_q)$ is given as:

$$G(z;\alpha,\sigma_q) = \exp\left[-\frac{(z-\alpha)^2}{2\sigma_q^2}\right] \tag{19}$$

where $\alpha = d/2$ and $\sigma_q = d/(2q)$. The quantity q is a tuning parameter for the apodization function.

In order to numerically analyze the spectral response of an apodized grating we proceed by specifying parameters for a volume grating designed for operation at 1.55 μm. We employ a transmission grating with a slant angle $\phi = 90^o$. The mean refractive index of the grating is $n_{20} = 1.5$ and amplitude of the modulated component of refractive index is $n_{21} = 0.64 \times 10^{-3}$. For convenience we set mean refractive indices in the bounding media to be the same as that of the grating: $n_{10} = n_{30} = 1.5$. We are interested in the grating's spectral response about the center wavelength $\lambda_0 = 1565$ nm. The angle θ_2 of the incident wave satisfies the Bragg condition:

$$\cos(\phi - \theta_2) = \frac{K}{2k_2} \tag{20}$$

In order to proceed further with our numerical solution we must specify the number of harmonics need to accurately represent the electric field. The number of spatial harmonics $M = M_2 - M_1 + 1$ is calculated from the minimum and maximum spatial harmonic indices M_1 and M_2 selected, where $M_1 \leq m \leq M_2$. The values of M_1 and M_2 required for an accurate representation of the solution can be gleaned by examining the eigenmodes of the homogeneous problem, where $f(z) = 1$. The solution to the homogeneous problem can be expressed as

$$S_m(z) = \sum_i C_i \Phi_{im} exp(\gamma_i z) \tag{21}$$

where γ_i is the i-th eigenvalue, Φ_{im} is the i-th element of the m-th eigenvector and C_i is one of a set of unknown coefficients determined by applying the boundary conditions in Eqs. (16-17). We find that increasing the number of spatial harmonics M produces modes that do not significantly contribute to the solution. For the grating parameters of interest here, we find that two spatial harmonics are sufficient to accurately describe the solution, *i.e.* $M_1 = 0$ and $M_2 = 1$.

The inhomogeneous coupled differential equations for $S_m(z)$ $\{M_1 \leq m \leq M_2\}$ are integrated by a solver that employs the numerical integrator `lsode` [12]. The standard `lsode` integrator solves initial value problems. A boundary value problem solver is fashioned by applying a shooting method in concert with `lsode`. The shooting method is used to adjust the estimated initial value at $z = 0$ so that the outputs of the `lsode` will satisfy the boundary conditions at $z = d$ with desired accuracy. The differential equations given in Eqs. (5-7) pose some difficulty for the integration code. For the optical parameters parameters of interest equations Eqs. (5-7) form a system of *stiff* [13] ordinary differential equations. The term *stiff* refers to a large disparity in the spatial scale of solutions admitted by the differential equations. A comparison of the magnitude of terms in Eqs. (5-7) reveals the highest derivative terms are $\mathcal{O}(1/d^2)$, while the lowest derivative terms are $\mathcal{O}(k_2^2)$. This difference in the magnitude of terms yields eigenvalues for the homogeneous problem ($f(z) = 1$)) that differ in magnitude by $\mathcal{O}(10^4)$. The consequence of this disparity is that the numerical integration of the differential equations requires step-sizes that adequately sample the fast spatial scale, albeit the dominant term in the solution corresponds to the slow spatial scale.

#5752 - $15.00 US Received 23 November 2004; revised 16 December 2004; accepted 16 December 2004

4. Approach for approximating Gaussian refractive index apodization in PTR glass

Lateral apodization can be performed by apodizing the intensity of recording beams. Apodization in the longitudinal direction relies on the photo-induced refractive index increment approaching saturation in a smooth manner. This allows for a two-step process where the primary exposure depletes the photo-sensitivity achievable in the secondary exposure. For example, a uniform holographic pattern can be generated by exposure with a transparent wavelength, while an apodizing exposure can be applied using a second absorbing wavelength. Dependence of induced refractive index increment for the cumulative exposure is described by a hyperbolic function as noted by Glebov previously [9]. We express the resultant refractive index increment achieved by with a two-exposure process by

$$\Delta n = \frac{\Delta n_{max} E}{\mathscr{E} + E}, \tag{22}$$

where Δn is the refractive index increment, E is the uniform hologram exposure energy in J/cm^2, Δn_{max} is the maximum refractive index increment, and $\mathscr{E}$ is the half-max dosage. Typical values of photosensitivity parameters for PTR glass are $\Delta n_{max} = 0.7 \times 10^{-3}$, $\mathscr{E}$ = 500 mJ/cm^2. The resultant refractive index increment in the presence of a background exposure, E_b, can now be expressed as

$$\Delta n = \Delta n_{max} \left(\frac{E_b + E}{\mathscr{E} + E_b + E} - \frac{E_b}{\mathscr{E} + E_b} \right). \tag{23}$$

Fig. 2 shows dependence of refractive index increment for the exposure at the hologram recording wavelength for different background exposure levels. These experimental results show that Δn can be varied by approximately an order of magnitude. The wavelength for ultraviolet exposure is usually chosen in the region of low absorption to provide a uniformity with depth. A background exposure can be applied using a shorter wavelength that experiences significant absorption within the photosensitive material. If such exposure is applied to both front (z=0) and back (z=d) surfaces then the distribution of absorbed energy along the longitudinal direction is

$$E_b = E_{bi} \left[\exp(-Az) + \exp(A(z-d)) \right] = E_{bi} B(z), \tag{24}$$

where E_{bi} is the incident background dosage and A is the absorption coefficient. We assume that photosensitivity does not depend on wavelength and no additional absorption occurs at the operational wavelength. Now, a substitution of Eq. (24) into Eq. (23) yields

$$\Delta n = \Delta n_{max} \left(\frac{E_{bi} B(z) + E}{\mathscr{E} + E_{bi} B(z) + E} - \frac{E_{bi} B(z)}{\mathscr{E} + E_{bi} B(z)} \right) \tag{25}$$

For a photosensitive plate of known thickness, varying the parameters of wavelength, background dosage level, and main dosage level afford a variety of spatial profiles in the refractive index increment. Fig. 3 shows that an approximation to the Gaussian profile in the refractive index increment can be achieved in a 4-mm thick photosensitive plate. This profile corresponds to an absorption coefficient of 6.4 cm^{-1} at a wavelength of 250 nm for PTR glass [5]. Illumination at this wavelength can be provided by a filtered Xe-lamp or by higher harmonics of visible or infrared lasers. This approach extends to lateral apodization which allows for fabrication of holograms with complex spatial profiles for the refractive index modulation.

#5752 - $15.00 US Received 23 November 2004; revised 16 December 2004; accepted 16 December 2004

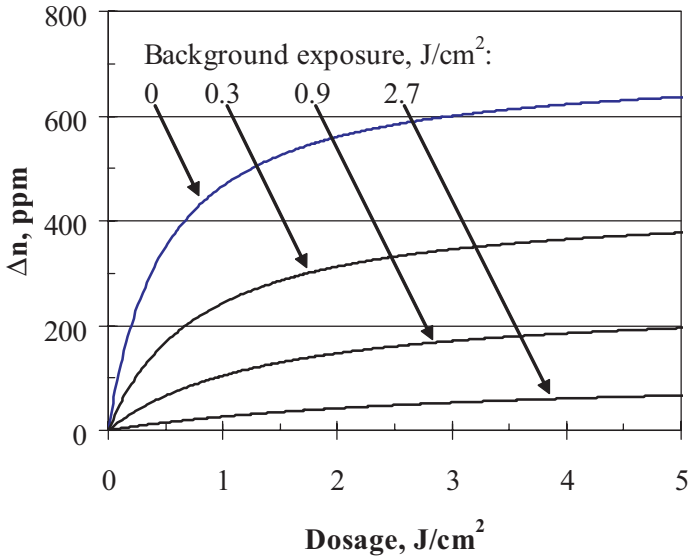

Fig. 2: Dependence of refractive index increment for the second exposure of PTR glass to UV radiation at 325 nm. Kinetics parameters are $\Delta n_{max} = 0.7 \times 10^{-3}$ and $\mathscr{E}$ = 0.5 J/cm^2.

5. Results

In this section we discuss the results obtained from the numerical solution of Eqs. (5-7), subject to the boundary conditions in Eqs. (16-17). We begin by examining the solution for a uniform grating ($f(z) = 1$). In Fig. 4 we present the variation in the magnitude of the diffracted order $S_1(d)$, with the grating thickness d. The coupling between spatial harmonics S_0 and S_1 results in a cyclical exchange of energy between the two modes as the grating thickness d increases. The value of $d = d_{max}$ at which $|S_1(d)|$ reaches its first maximum indicates the interaction length required for maximum diffraction efficiency. A grating of thickness d_{max} acts as a band-reject filter for S_0 (the reference wave) such that a selected band of wavelengths about λ_0 are rejected and all others are passed. For S_1 (the diffracted wave) the grating acts as a band-pass filter which transmits a band of wavelengths about λ_0 and rejects wavelengths outside the passband. In Fig. 5 we present the response of $S_0(d_{max})$ and $S_1(d_{max})$ as a function of λ. This figure compares numerically computed results with experimental measurements of a uniform grating device. We perform this comparison to validate our numerical model. A grating written in photothermorefractive glass [5, 6] is employed for our experimental measurements. For the experiment, a beam from a tunable laser, collimated to a 12 mm $1/e^2$-diameter, was incident on the grating at the Bragg-matching angle of incidence. Optical power meters were placed on each side of the grating to measure the reference and diffracted intensities. The power meters were positioned to measure the S_0 and S_1 diffracted orders. The laser was tuned over wavelengths from 1555 to 1575 nm to measure the dependence of $|S_0|^2$ and $|S_1|^2$ versus λ. The experimental spectral response of the grating is found to closely match the numerically computed response, as shown in Fig. 5. The spectral response for $|S_1(d_{max})|^2$ exhibits a passband centered at $\lambda =$ 1565 nm and an envelope of $|S_1(d_{max})|^2$ that decays by approximately -20 dB over 15 nm as seen in Fig. 5.

#5752 - $15.00 US Received 23 November 2004; revised 16 December 2004; accepted 16 December 2004

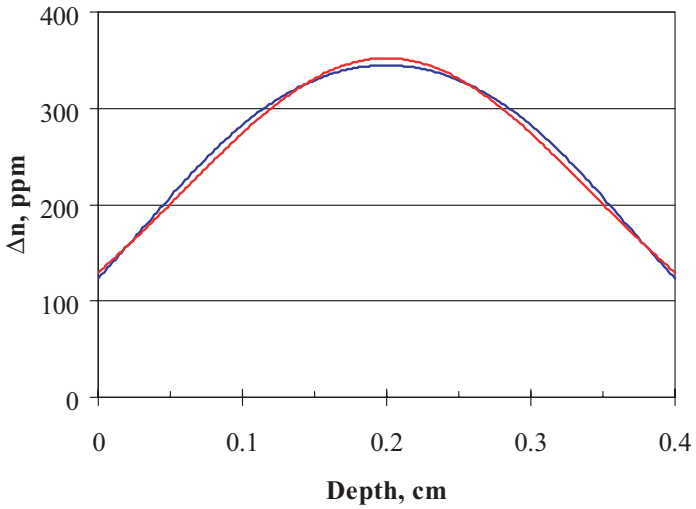

Fig. 3: Distribution of refractive index increment in depth of PTR glass after two step exposure to UV radiation at 325 and 250 nm with dosages of 0.7 and 0.6 J/cm^2, respectively. The red line is a Gaussian function with half-width of 0.2 cm.

To develop gratings with sharper rolloff, we now examine the results for apodized gratings which are computed through the numerical solution of an inhomogeneous problem. Fig. 6 shows the variation in the magnitude of the diffracted order S_1 as function of d for $f(z) = G(z, \alpha, \sigma_q)$, with $\{q = 1 \ldots 4\}$. For convenience we denote $G(z, \alpha, \sigma_q)$ by G_q. We note that the coupling strength between the reference and the diffracted orders near the grating boundaries is reduced as the value of apodization tuning parameter q is raised. The presence of apodization slows the exchange of energy between the reference and diffracted orders, requiring a longer interaction length to achieve maximal diffraction efficiency. The spectral response of S_1, for a set of tuning parameters $\{q = 1 \ldots 4\}$ is plotted in Fig. 7. The results are compared with the spectral response for the case $f(z) = 1$. For each spectral response plotted in Fig. 7, the value d_{max} corresponds to the thickness at which $|S_1|^2$ reaches a maximum. The results in Fig. 7 show a progressively greater suppression of the stop-band response for increasing q. In the case of $q = 4$, the first and second-order side-lobe peaks are further reduced by 33 and 65 dB, respectively, yielding a stop-band rejection exceeding 80 dB at $\lambda_0 \pm 15$ nm.

6. Summary and conclusions

In this work we have presented the use of apodization for enhancing the stop-band rejection of volume gratings. We have followed a rigorous approach in our analysis for the problem of plane wave diffraction by apodized gratings. The analysis yields a set of inhomogeneous coupled-wave differential equations that govern the spatial variation of the electric field in the grating. We have developed a numerical approach to compute the solution of this set of coupled differential equations. This numerical model has been confirmed by measurements of an experimental uniform volumetric grating in photothermorefractive glass.

Using our numerical approach, we have computed the spectral response of volume gratings for a set of Gaussian apodization profiles. Our results have shown that such apodized gratings can achieve high diffraction efficiency for thicknesses under 4 mm. Recent experimental efforts suggest that gratings with thicknesses of 5 mm with n_{21} of $\mathcal{O}(10^{-3})$ are realizable in photother-

#5752 - $15.00 US Received 23 November 2004; revised 16 December 2004; accepted 16 December 2004

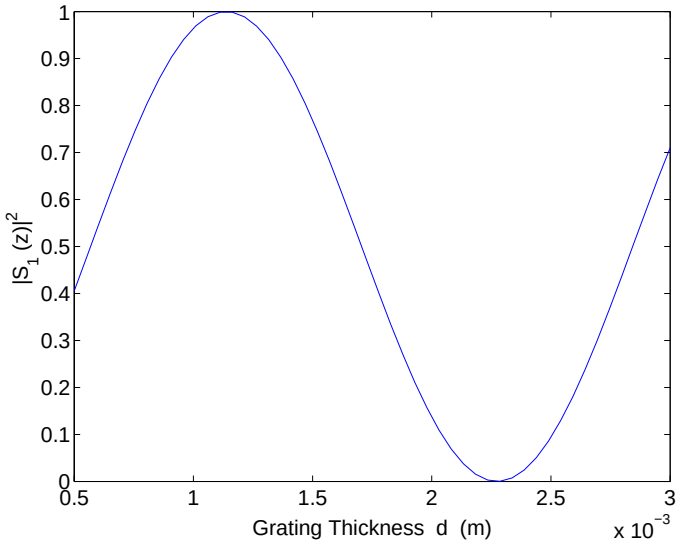

Fig. 4: $|S_1|^2$ as function of d for $f(z) = 1$ and $d_{max} = 1.15$ mm.

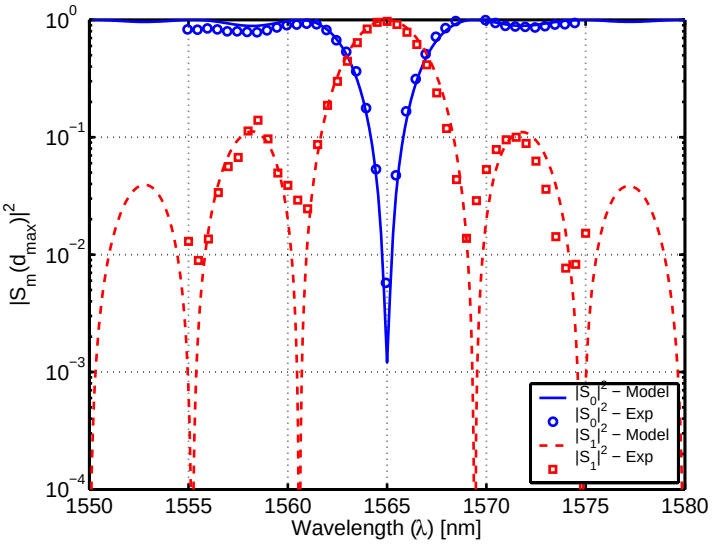

Fig. 5: The spectrum of $|S_0(d_{max})|^2$ and $|S_1(d_{max})|^2$ for $f(z) = 1$.

#5752 - $15.00 US Received 23 November 2004; revised 16 December 2004; accepted 16 December 2004

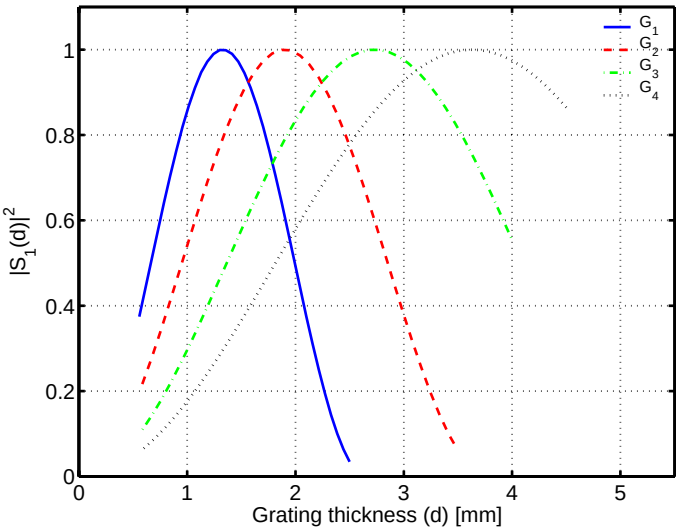

Fig. 6: $|S_1|^2$ as function of d for $f(z) = G_q$, with $q = 1 \ldots 4$.

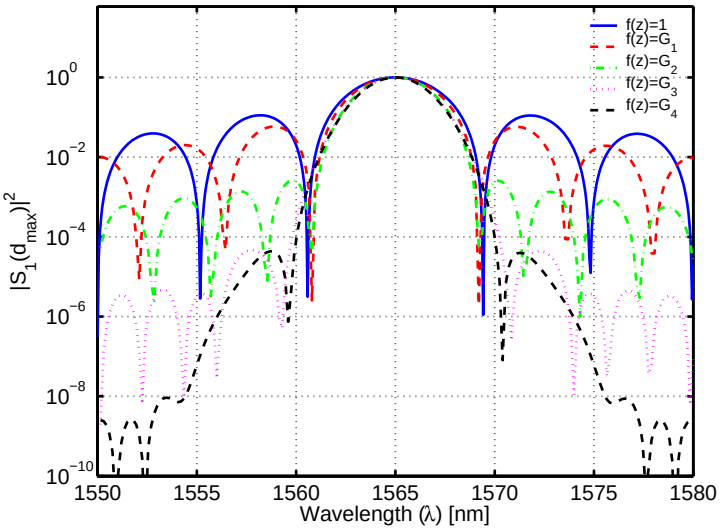

Fig. 7: The spectrum of $|S_1(d_{max})|^2$ for uniform and apodized gratings.

#5752 - $15.00 US Received 23 November 2004; revised 16 December 2004; accepted 16 December 2004

morefractive glass. We have shown significant suppression of side-lobe peaks while preserving the main-lobe shape. This feature provides new opportunity for the use of volume grating-based devices in applications requiring high spectral selectivity.

Acknowledgments

This work was sponsored by the Department of the Air Force under Contract F19628-00-C-0002 and DARPA under contract HR-01-1041-0004. Opinions, interpretations, conclusions, and recommendations are those of the author and are not necessarily endorsed by the United States Government.

#5752 - $15.00 US Received 23 November 2004; revised 16 December 2004; accepted 16 December 2004